

UAV Icing: A Performance Model for a UAV Propeller in Icing Conditions

Nicolas C. Müller*, Richard Hann†

Norwegian University of Science and Technology, NTNU, Trondheim, Norway
UBIQ Aerospace AS, Trondheim, Norway

In-flight icing on unmanned aerial vehicles is a severe hazard and imposes limits on the operational envelope. Icing has been shown to lead to substantial aerodynamic performance losses on lifting surfaces and propellers. To quantify the performance loss of the propeller in icing conditions, this study proposes a model that describes the performance of a fixed-wing UAV propeller in icing conditions. For the development of this model, experiments in an icing wind tunnel have been performed to evaluate the performance loss of the propeller in different icing conditions. From the thrust and torque measurements, a model for the transient performance of a propeller in icing conditions has been developed. The model calculates thrust and torque as a function of the temperature, liquid water content, advance ratio, and the rotation rate of the propeller. This model contains an estimator for the ice accumulation on the propeller, the ice shedding forces of the propeller, and the performance of the iced propeller. This model can for example be used to estimate the flight performance of UAVs in icing conditions. It could also be applied for path and mission planning tools, autopilot, flight simulators, performance-based ice detection and the design of ice protection systems.

I. Introduction

UNMANNED aerial vehicles (UAVs) also called unmanned aerial systems (UAS) are an emerging technology that faces many challenges. One particular operational challenge is adverse weather that poses a threat to UAVs. One of these adverse weather conditions is in-flight icing. In-flight icing is a very frequent scenario [1] in large areas of the world. In-flight icing occurs in meteorological conditions where supercooled liquid water exists in the atmosphere. When these supercooled droplets collide with the airframe, they freeze and accumulate over time. The resulting ice accretions can lead to severe aerodynamic performance penalties, especially on unmanned aircraft [2]. Icing is also a hazard to manned aircraft [3] but is a relatively mature research field nowadays. In contrast, icing is an emerging research topic for unmanned aircraft with its earliest mention in the 1990s [4]. Since then, several studies have been conducted to investigate the negative effects of icing on UAVs. The majority of these studies use numerical or experimental methods to evaluate the aerodynamic penalties on airfoils and wings [5–8]. The existing literature shows that ice has severe negative effects on lifting surfaces, typically leading to a decrease in the lift, increase in the drag, and reduction of stall angles.

The effect of in-flight icing on UAV propellers has even more recently come into the focus of research. Several experimental and numerical studies have shown that icing leads to a very rapid decrease in thrust and performance efficiency whereas torque is substantially increased [9–11]. The literature suggests that propeller icing leads to faster and more severe performance penalties compared to icing on lifting surfaces. Therefore, propeller icing is a significant threat to UAV operations and deserves in-depth investigations. The existing research on the icing on propellers is focused on the icing on multi-rotor propellers [12]. In this paper, an effort has been made to predict the time-dependent change in the performance of the propeller and to include it in a flight performance model. The performance degradation is captured as a linear performance degradation over time [12].

In this work, experiments are performed to analyse the performance of a propeller of a UAV in icing conditions. The propeller is tested in an icing wind tunnel (IWT) at multiple different temperatures and rotation rates, to create a database of experimental results to parameterize a propeller performance model. The novelty of this work is replacing the time dependency with an ice accretion factor, which allows scaling of the results for different icing conditions, rotation rates and flight velocities. The performance degradation model can be coupled with a propeller polar model which allows the use of the model for the calculation of the flight performance of a UAV in multiple flight conditions.

*PhD candidate, Centre for Autonomous Marine Operations and Systems, Department of Engineering Cybernetics, NTNU

†Researcher, Centre for Autonomous Marine Operations and Systems, Department of Engineering Cybernetics, NTNU

The objective of this study is to develop a model to estimate the performance of fixed-wing UAV propellers in clean and icing conditions. The model is based on experimental data that was obtained from icing wind tunnel tests on a typical fixed-wing UAV propeller. The model estimates the thrust and torque of the propeller as a function of the temperature, advance ratio, liquid water content, and icing duration. The model consists of three submodels. The clean performance model for the estimation of the clean performance. The ice accretion model estimates the amount of ice on the propeller. Finally, the iced performance pert will estimate the performance of the propeller with the ice accumulation.

In this model, the correlation between the thrust, the power coefficients, and the advance ratio is calculated using a second-order polynomial approximation. The performance change due to icing is calculated as a correction factor to the model coefficients. The model also accounts for ice shedding. This describes the process of parts of the accumulated ice breaking off the propeller. The model can be used to calculate the maximum amount of ice that can accumulate on the propeller. The proposed model offers an important contribution to understanding and dealing with the UAV icing challenge. Predicting icing performance losses in icing conditions for propellers is a key element to develop path-planning and mission-planning tools [13, 14]. Furthermore, the model helps identify the most hazardous icing conditions which is an important design aspect for ice protection systems [15, 16]. The calculated performance data can also be used to train autopilots for flights in icing conditions. It can also be used to predict the performance impact of a flight through icing conditions, which can be used to calculate the optimal flight path through clouds with possible icing conditions. Last but not least, the proposed performance model is useful for flight simulators and modelling of flight behaviour in icing conditions [17]. The collected dataset of propeller performance measurements can be used to calculate the severity of different icing conditions for UAVs [18].

II. Methods

In this section, the methodologies used for this study are presented. First, the equations to derive the experimental data are shown, then the experimental methods and then the model created out of the data will be presented.

A. Test Setup

The measurements for this paper have been performed in an icing wind tunnel at the VTT Technical Research Centre of Finland in Helsinki [19]. This icing wind tunnel has a test section with a width and height of 70 cm and allows for testing with wind speeds of up to 50 m/s. For the test, a propeller that is representative of a fixed-wing UAV with a wingspan of 3 meters was chosen. The chosen propeller is the "Propeller 21x13 CCW 2B E" manufactured by Mejzlik Propellers sro [20] and has a radius of 0.53 m and a pitch of 0.33 m. An RC-Test bench 1780 from Tycho robotics [21] is used to measure the thrust and the torque of the propeller and to control the speed-controller. The rotation rate of the propeller is measured using an optical sensor and a reflector on the motor. A custom made conical cover protects the motor and the force measurement areas from ice. This cover is not connected to the force measurement unit. An Axi 5345 HD 3D Extreme V2 motor is used with a Hacker Master Spin-99 Opto speed controller. The motor rotation rate is kept constant with a PI controller in a Javascript script. A Phantom VEO 710L high-speed camera is triggered by the signal from the optical rotation rate sensor and takes an image of a propeller blade during each rotation. Four MultiLED QT lights are used to illuminate the propeller for the images of the high-speed camera and are controlled by a MultiLED G8 controller. It uses the signal from the optical sensor to switch on the lights synchronous with the high-speed camera. To avoid excessive heat influx into the propeller the lights are only illuminated for 15 μ s per rotation. Therefore only a maximum of 0.3% of the rotation of the propeller is illuminated, preventing any influence of the light on the ice accretion on the propeller. The liquid water content (*LWC*) of the wind tunnel is calibrated at the beginning of each experimental test campaign using a rotating cylinder [22].

1. Testing Procedure

The testing procedure started with the start of the wind and the motor. Both were given 30 s to stabilise before the spray system was switched on and the ice accretion time started. Multiple experiments were performed with icing durations between 60 s and 600 s.

To assess the performance of the propeller in icing conditions, three different tests have been performed. The first is a test where the propeller is operated at a constant rotation rate and a constant velocity of the air in the wind tunnel. This enables the time dependency of the performance of the propeller. Additional tests are performed by creating a polar of the propeller in clean and in icing conditions. For this test first, a constant velocity of the air stream is selected. Then

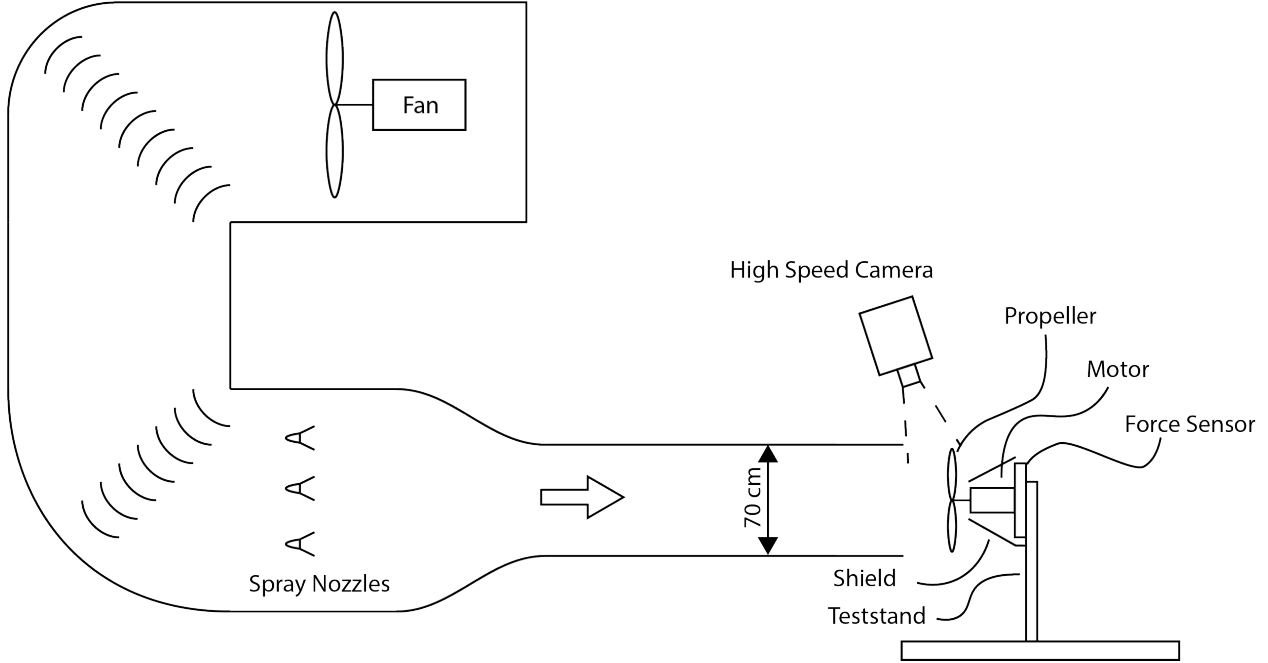


Fig. 1 Experimental setup at the icing wind tunnel at the VTT facilities in Helsinki.

the propeller is operated across its entire performance spectrum. During this test, the performance of the propeller for different advance ratios has been calculated. For the last test, the ice shedding from the propeller is estimated. To measure the time of the ice shedding, the propeller is run at different rotation rates and the time of the first ice shedding event is noted. The timing of ice shedding events is derived from the change of the thrust measured. This allows for the analysis of the influence of the rotation rate on the timing of the ice shedding.

2. Testing Conditions

The propeller was tested under different conditions to cover the range in which the propeller was used. The temperature range was in a range from $-2\text{ }^{\circ}\text{C}$ to $-20\text{ }^{\circ}\text{C}$. The wind speed varied from 10 m/s to 25 m/s. The rotation rate varied from 1750 1/min to 5200 1/min. A data set of 58 performance tests with constant rotation rates was used for the development of the data. This led to at least five measurements for each temperature except for $-2\text{ }^{\circ}\text{C}$, which has only 2 measurements. With this large data set of propeller measurements, it was possible to analyse the impact of icing on the performance of the propeller over its entire performance range.

B. Clean performance model

The clean performance model is based upon the general equations for the performance of a propeller. The thrust can be calculated according to [23]. Here the thrust coefficient C_T is defined as a dimensionless value derived from the thrust T , the rotation rate n , the diameter of the propeller d and the air density ρ .

$$C_T = \frac{T}{\rho n^2 d^4} \quad (1)$$

The advance ratio J is used as a factor describing the relation between the forward airspeed of the UAV v_{∞} and the rotation rate of the propeller. This parameter can be used to describe the airflow characteristics over the propeller and can be used as a comparison tool to compare propellers of different diameters or at different airspeed [23].

$$J = \frac{v_{\infty}}{n d} \quad (2)$$

To capture the variations of the thrust coefficient with the advance ratio, a polynomial approximation of the second-order is used, which is derived from Coates et al. [24] in Eq. 3. Here three factors $C_{T,0}$, $C_{T,1}$ and $C_{T,2}$ are used

to create an analytical approximation of the thrust coefficient.

$$C_T(J) = C_{T,0} + C_{T,1} J + C_{T,2} J^2 \quad (3)$$

The power P and the power coefficient C_P can be calculated according to [23].

$$C_P = \frac{P}{\rho n^3 d^5} \quad (4)$$

The coefficients are also dependent on the advance ratio and approximated by a second-order polynomial approximation according to Coates et al.[24] in Eq. 5. Here three factors $C_{P,0}$, $C_{P,1}$ and $C_{P,2}$ are used to create an analytical approximation of the power coefficient.

$$C_P(J) = C_{P,0} + C_{P,1} J + C_{P,2} J^2 \quad (5)$$

C. Ice accretion model

The ice accretion model is used to approximate the influence of the ice accretion on the performance of the propeller. Therefore the thrust coefficients are now also dependent on the temperature T , the icing time t , the LWC and the median droplet diameter MVD .

$$C_{T,ice} = C_T(T, t, LWC, J, MVD) \quad (6)$$

$$C_{P,ice} = C_P(T, t, LWC, J, MVD) \quad (7)$$

For the influence of the advance ratio, the assumptions for the clean propeller are used. To estimate the influence of the ice accretion on the performance of the propeller, the factors $C_{T,0}$, $C_{T,1}$, $C_{T,2}$, $C_{P,0}$, $C_{P,1}$ and $C_{P,2}$ are modified to accommodate the change in the performance. This is done on the thrust and the power coefficient, but if required the data from the power coefficient can easily be transformed into torque coefficient values.

For the dependency on the time and the LWC , the icing rate is used. To describe the icing rate, a factor for the total water collection (TWC) is used which combines the time and the LWC according to Eq. 8. All data is shown for the ice accretion on the propeller after 60 s and an LWC of 1 g/m^2 .

$$TWC = t LWC \omega \frac{d}{2} \quad (8)$$

An important factor for the icing on the UAV is the ice shedding from the propeller. To calculate the time at which the ice is shedding from the propeller, the adhesion forces of the ice to the surface were used. These forces are dependent on the temperature, surface roughness and icing type [25]. For this study, the surface roughness is assumed to be constant for the propellers, so the main focus is on the temperature dependency. The forces acting on the ice on the propeller are the centrifugal forces caused by the rotation of the propeller and the aerodynamic forces created by the airflow, as well as the adhesion forces between the ice and the propeller. The relative airspeed caused by the airspeed of the UAV is an order of magnitude lower than the airspeed induced by the rotation of the propeller and has been neglected in the study. This leaves the aerodynamic forces caused by the rotation of the propeller. The aerodynamic forces are proportional to the stagnation pressure. The second force is the centrifugal force acting on the ice. Both forces scale with the second-order of the relative airspeed [26], which is proportional to the rotation rate. So the strain A_{max} is introduced in Eq. 9, which represents the adhesion forces of the ice on the propeller. They are calculated dependent on the amount of water collected on the propeller at the moment of the ice shedding $TWC_{shedding}$, the diameter d and the rotation rate of the propeller ω . In an ideal case without aerodynamic forces and cohesion forces radial along with the propeller, this would represent the required adhesion forces to prevent the ice shedding. The values at the tip are used since the ice shedding is starting from the tip. The dependency of the ice shapes on the aerodynamic forces is not explicitly included, but since the ice shapes are dependent on the temperatures, they can be included when this value is calculated for different temperatures.

$$A_{max} = TWC_{shedding} \frac{d}{2} \omega^2 \quad (9)$$

This factor is used to evaluate the adhesion forces dependent on the temperature, the material and the surface properties of the propeller. It can additionally be used to predict the maximum amount of ice on the propeller to calculate the amount of ice that accumulates on the propeller before ice shedding is expected. This is shown in Eq. 10

$$TWC_{\max} = \frac{A_{\max}}{\frac{d}{2} \omega^2} \quad (10)$$

In Fig. 2 the ice shedding for a case at -15°C is shown. The ice sheds from the propeller in multiple ice shedding events. First, the ice on the tip of the propeller is shed, and then the ice closer to the center is shed later after more ice has collected on the propeller. For each subsequent ice shedding event, the radius of the propeller until which the ice remains on the propeller is shrinking. After the ice has shed from one section it will start to accumulate more ice until the ice mass has crossed a threshold and it is shedding again. In this paper, the prediction focused on the ice shedding on the tip of the propeller. Here the ice shedding is dependent on the adhesion forces between the ice and the propeller and the cohesion forces along the radius of the propeller. The ice on areas closer to the middle of the propeller will hold the ice on the propeller on sections further out until the maximum cohesion and adhesion stresses are reached and the ice sheds off the propeller. Compared to the adhesion forces, the cohesion strength of the ice is not strongly dependent on the temperature [27, 28], so it can be assumed to be proportional to the area of the ice. Therefore the cohesion forces and the adhesion forces were combined into one parameter that describes the adhesion of ice on the propeller. The ice type will have a big influence on the ice shape and thus on the ice adhesion, beyond the strength of the connection itself. The ice shape itself is very temperature-dependent.

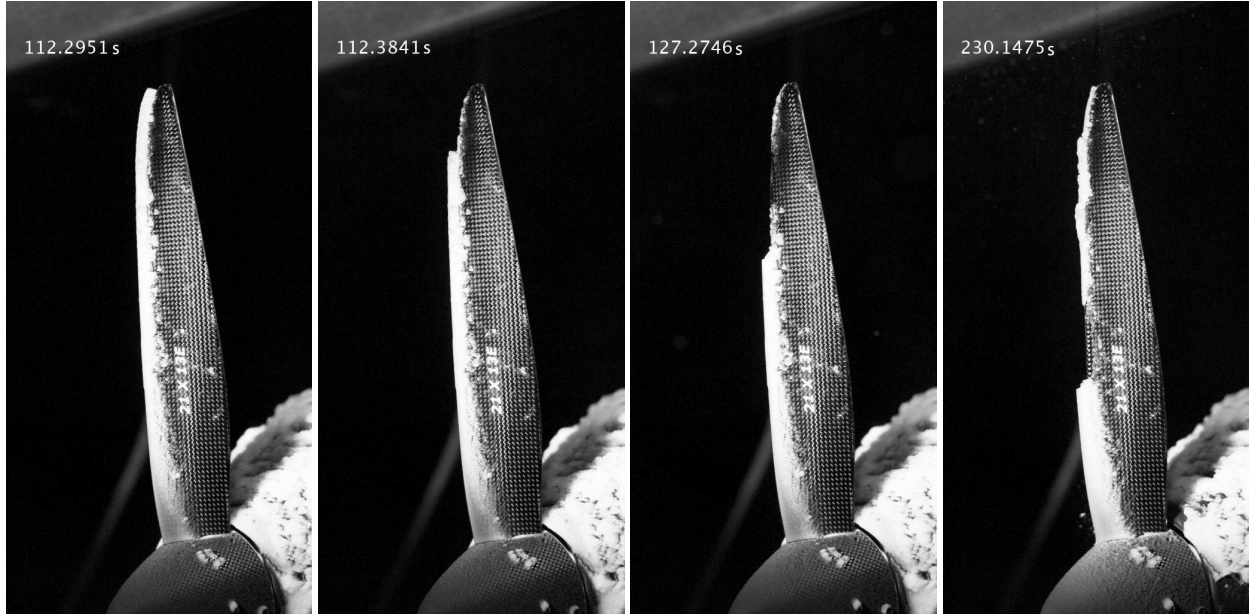


Fig. 2 Ice shapes on the propeller during an icing run at -15°C showing ice on the propeller before and after ice shedding events.

For the influence of the temperature on the thrust and performance degradation, another quadratic model can be used for the calculation of the performance degradation of the propeller, as well as for the estimation of the TWC_{\max} . This parameter is dependent on the adhesive force that exists between the propeller surface and the ice. For this model, the aerodynamic forces on the ice are ignored and only the centrifugal forces are observed, leading to an inverse proportional relationship between the time and the rotational rate. Therefore, the total set of equations for the thrust model consists of the Eqs. 11, 12, 13 and 14.

$$C_T(T, TWC) = C_T(J) * (1 + \min(TWC, TWC_{\max}) * \Delta C_T(T)) \quad (11)$$

$$\Delta C_T(T) = \Delta C_{T,0} + \Delta C_{T,1} T + \Delta C_{T,2} T^2 \quad (12)$$

$$A_{\max}(T) = A_{\max,0} + A_{\max,1} T^2 \quad (13)$$

$$TWC_{\max}(n) = \frac{A_{\max}}{2 d n^2 \pi^2} \quad (14)$$

The equivalent is performed for the power coefficient:

$$C_P(T, TWC) = C_P(J) * (1 + \min(TWC, TWC_{\max}) * \Delta C_P(T)) \quad (15)$$

$$\Delta C_P(T) = \Delta C_{P,0} + \Delta C_{P,1} T + \Delta C_{P,2} T^2 \quad (16)$$

$$C_P(J) = C_{P,0} + C_{P,1} J + C_{P,2} J^2 \quad (17)$$

III. Results

A. Clean performance data

In the following, the parameters are shown for the Mejzlik 21x13E propeller. The source of the data for the performance of the ice-free propellers is provided by Mejzlik, obtained through a separate wind tunnel experiment out of the scope of this paper. The thrust and the power polar were recorded by keeping the propeller spinning at a rotation rate of 4800 revolutions per minute and by varying the wind speed in the wind tunnel. This kept the Reynolds number constant across the experiment.

The recorded measurements were used to calculate the clean performance model. First, all the points with a negative advance ratio are discarded, to limit the model to the propeller conditions relevant for the flight of a fixed-wing UAV. Then a polynomial fit with the least-squares condition was performed on the remaining data points. The results for the thrust coefficient can be seen in Fig. 3. Comparing the experimental data with the approximation in the model, a good agreement can be found at an advance ratio of 0.2 and above. The model parameters used for the model can be seen in Table 1. The experimental results for the power coefficient can be seen in Fig. 4, with the approximation factors presented in Table 2. Here the model provides a good approximation for advance ratios above 0.3.

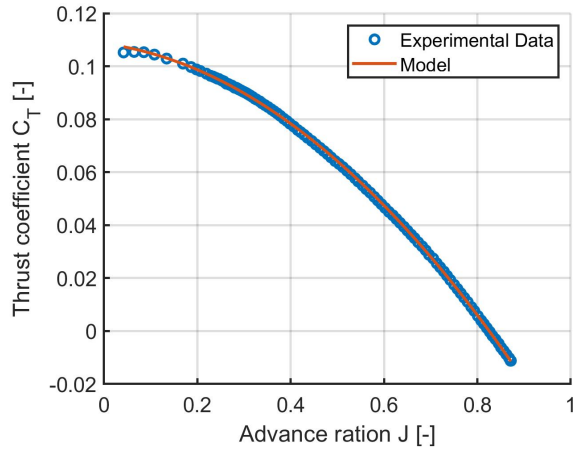


Fig. 3 The thrust coefficient of the Mejzlik 21x13E propeller over the advance ratio with the approximated values from a polynomial fit as used in the propeller performance model.

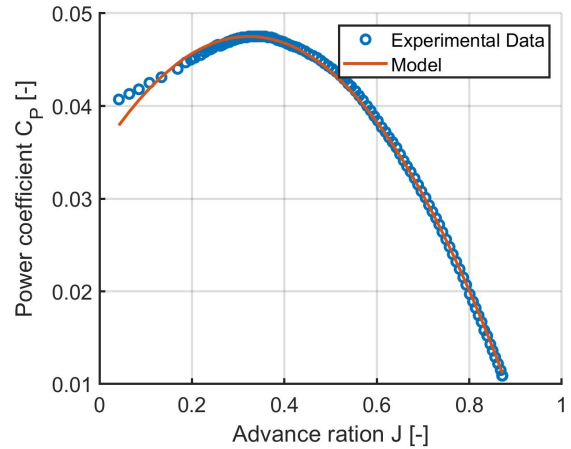


Fig. 4 The power coefficient of the Mejzlik 21x13E propeller over the advance ratio with the approximated values from a polynomial fit as used in the propeller performance model.

Table 1 Parameters used for the estimation of the thrust coefficient of the Mejzlik 21x13 E propeller.

Parameter	Value [-]
$C_{T,0}$	0.109
$C_{T,1}$	-0.0230
$C_{T,2}$	-0.131

Table 2 Parameters used for the estimation of the power coefficient of the Mejzlik 21x13 E propeller.

Parameter	Value [-]
$C_{P,0}$	0.0348
$C_{P,1}$	0.0782
$C_{P,2}$	-0.121

B. Icing wind tunnel data overview

The testing of the performance of the propeller in an icing wind tunnel revealed a very quick degradation of the performance of the propeller. In Fig. 5 the efficiency of the propeller compared to the clean configuration can be seen. The spray system is activated at a timestamp of 0s. After the spray system is started, ice starts to accumulate on the propeller. This is indicative by the reduction of the relative efficiency of the propeller. When enough ice has accumulated on the propeller, it will start to shed off, this is indicated on this plot by a sudden increase in the efficiency of the propeller.

Figure 5 shows that the temperature has a significant influence in the rate of the performance degradation and the time of the first ice shedding event. The gradient of the performance loss appears to be correlated to the temperature, with the fastest performance loss rate at $-10\text{ }^{\circ}\text{C}$. At lower temperatures, the performance degradation curve is not as steep, also at higher temperatures. Also, a correlation between the time for the ice shedding and the temperature is visible. Here lower temperatures seem to lead to an earlier ice shedding, while the ice shedding seems to occur later at higher temperatures. The maximum performance loss of the propeller is dependent on the time at which the ice shedding occurs.

For selected icing conditions, a performance polar was created. In this polar the performance of the propeller is measured over the advance ratio. For this propeller polar the airspeed of the icing wind tunnel was kept constant and the rotation rate was increased. This was performed on a propeller before the first ice shedding event has occurred. In Fig. 6 the thrust and power polar of the propeller are shown for a condition after 60 s of icing at $-10\text{ }^{\circ}\text{C}$ and a rotation rate of 5100 revolutions per minute. A comparison between the iced and the ice-free propeller shows that the gradient of the thrust coefficient is steeper for the ice-free propeller, which indicates that the ice-free propeller can create more thrust for a given condition than the iced propeller. Both lines intersect at the advance ratio of 1 and a C_T of 0, the point at which the propeller changes from producing thrust to producing drag because it is actively turned by the airflow. The power coefficient shows a different behaviour, where the power coefficient of the iced propeller is always higher than the ice-free propeller. The point at which the iced propeller requires no power to turn is moved to a higher advance ratio, indicating that the propeller is producing more drag even if no lift is produced. The fact that the power coefficient is closer to the iced propeller at low advance ratios could be explained by the larger induced drag of the ice-free propeller due to its higher lift under those conditions compared to the iced propeller.

C. Ice Shedding analysis

For the estimation of the maximal ice accretion time, until the ice shedding occurs, the data from the wind tunnel experiments in Finland is used. The ice shedding was detected on the high-speed camera as well as on the force measurement unit. The ice shedding is visible as an increase in the thrust of the propeller and a decrease in the required mechanical power of the propeller. For each run, the ice shedding time was analysed from the data. An ice shedding event is detected when the efficiency of the propeller increases by a fixed amount that is dependent on the temperature. For temperatures of $-15\text{ }^{\circ}\text{C}$ and below, a threshold of 5% is used, at $-10\text{ }^{\circ}\text{C}$ a threshold of 2.50% is used and at higher temperatures, a threshold of 1.25% is used. This reflects the larger amount of ice shed at the lower temperatures. This is due to the longer ice accretion time until the ice is shed. With this data, the ice shedding at different temperatures can be shown.

The main parameter for the A_{\max} is the time until the ice sheds from the propeller. To create an approximation of the values of the maximum adhesion force A_{\max} for each temperature, the factor A_{\max} was calculated for every test run. Runs without ice shedding were not regarded as only the lower bound of the ice shedding time is known. An example of the extraction can be seen in Fig. 7. Here the detected ice shedding times are highlighted with dashed red lines. It

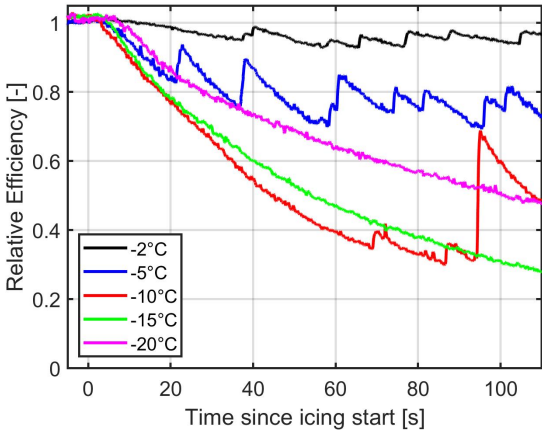


Fig. 5 Efficiency of the propeller in icing conditions with an rotation rate of 3500 1/min, an LWC of 0.44 and a wind velocity of 17 m/s.

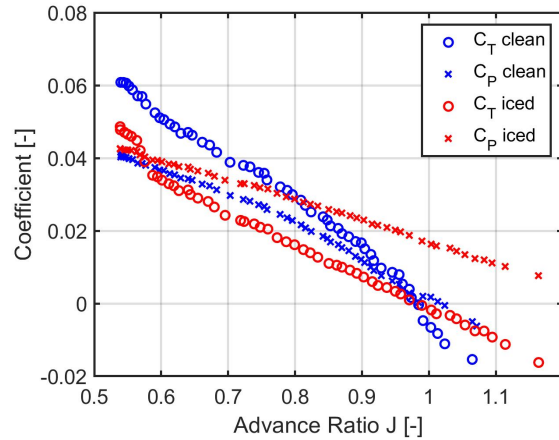


Fig. 6 Propeller polar after 60 s icing time at an LWC of 0.44 g/m³ and a wind velocity of 17 m/s at an rotation rate of 3500 1/min.

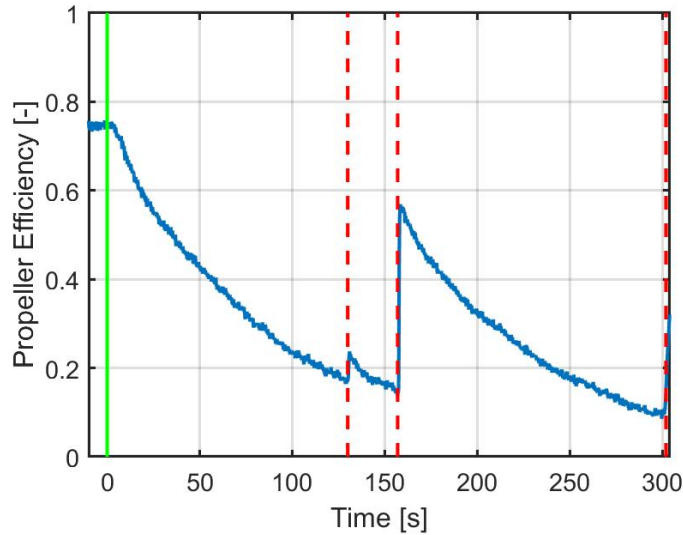


Fig. 7 Ice shedding analysis on the propeller at $-20\text{ }^{\circ}\text{C}$ at an 4200 1/min an airspeed of 25 m/s and an LWC of 0.45 g/m³. Ice shedding events are marked with a red dashed line, the green line represents the spray system activation.

can be seen, that a small ice shedding event was detected after 130 s, and a stronger one after 157 s. In the following analysis, always the first ice shedding event is used for the analysis.

In Figure 8 the adhesion force at the moment of the first shedding event is visualised. A total of 58 data points were extracted from the experiments. This allows for more than 5 data points for each temperature except for $-2\text{ }^{\circ}\text{C}$, which has only two valid data points. The data shows that the adhesion forces are growing with a decrease in the temperatures. To estimate the evolution of the adhesion force with the temperature, it was assumed that the ice adhesion forces have a parabolic shape that would be symmetrical around the freezing point. This leads to an estimation of the adhesion force according to the approximation $A_{max} = aT^2 + b$. This equation was fit to the experimental results using the least-squares method and lead to the estimations of $a = 1223$ and $b = 37.250$. This estimation is shown in Fig. 8 as a red line.

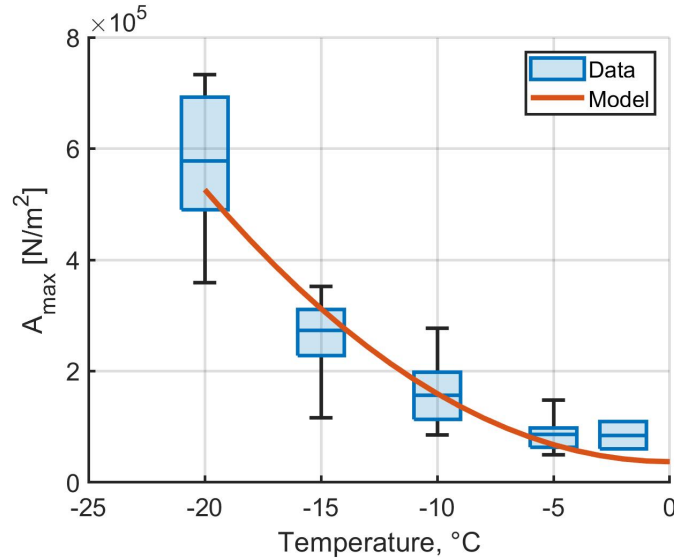


Fig. 8 Maximum estimated adhesion of the ice on the propeller for plotted over multiple temperatures.

D. Change in the performance

The ice shape geometries are different and dependent on the temperature. At temperatures close to the freezing point, the ice type is general glaze ice. If the rotation rate is below 2000 1/min and allows for a significant ice accretion on the leading edge, the ice shows complex ice shapes made of horns and lobster-tails [29]. For higher rotation rates, the ice on the leading edge will shed rapidly, and only some ice accretion can be seen on the pressure side of the propeller. For temperatures at -10 °C and lower, a larger ice shape will form on the leading edge. This ice shape will show different ice morphologies, going from glaze ice at -5 °C to a rime ice shape at -20 °C. In Fig. 9 the ice on the propeller after 60 s of icing is shown for the propeller at -5 °C, -10 °C, -15 °C and at -20 °C. At -5 °C, a glaze ice shape is visible and it is obvious that an ice shedding event occurred before the image was taken. At the lower temperature, the ice shape starts to more closely represent a streamwise shape, with a continuous increase in the smoothness of the ice shapes. At -20 °C, the most streamwise ice shape is visible. This can be seen by the increase in the icing extend on the propeller, which could be caused by the fact that at -10 °C and -15 °C the ice grows from the leading edge is creating horns, which reduces the impingement further down the propeller. The ice shapes on the propellers are dependent on the stagnation temperature. Due to the relative airspeeds at the tip of the propeller reaching up to 130 m/s, the stagnation temperature on the tip of the propeller is higher than the ambient air temperature. Because the most significant icing on the propeller has been observed at temperatures of -10 °C and below, this effect was not included in this paper.

To estimate the change in the performance of the propellers, the evolution of the thrust and the power coefficients of the propeller was analysed for the time frame between the start of the icing and the ice shedding. To remove the influence of small changes in the time the spray system is activated, the first 5 seconds of icing are not used. Similarly, the last five seconds before an ice shedding event are not used for the prediction of the performance, to avoid the influence of small ice shedding events that come before the main ice shedding event could have on the performance of the propeller. In Fig. 10 the plots for the thrust coefficient and the power coefficient for one test run are shown. Here the linear fitted curves are included as dashed lines. The linear approximation is fitting very well during the main part of the performance degradation. Both the thrust and the power coefficients drop in the initial stages of the ice accretion. This drop does not affect the efficiency of the propeller since thrust and power drop uniformly.

For the ΔC_T and ΔC_P calculation, the thrust loss of the experimental runs was calculated. For the calculation of the gradient, the time since the ice accretion was converted in the TWC of the propeller to compare runs with different conditions. Only runs with more than 10 seconds for the evaluation of the gradient were used. The reference value is taken from before the start of the spray system of the wind tunnel and averaged over 10 seconds. The LWC and the rotation rate of each experimental run were used to calculate the TWC . For each run, the gradients were calculated and plotted over the temperature.

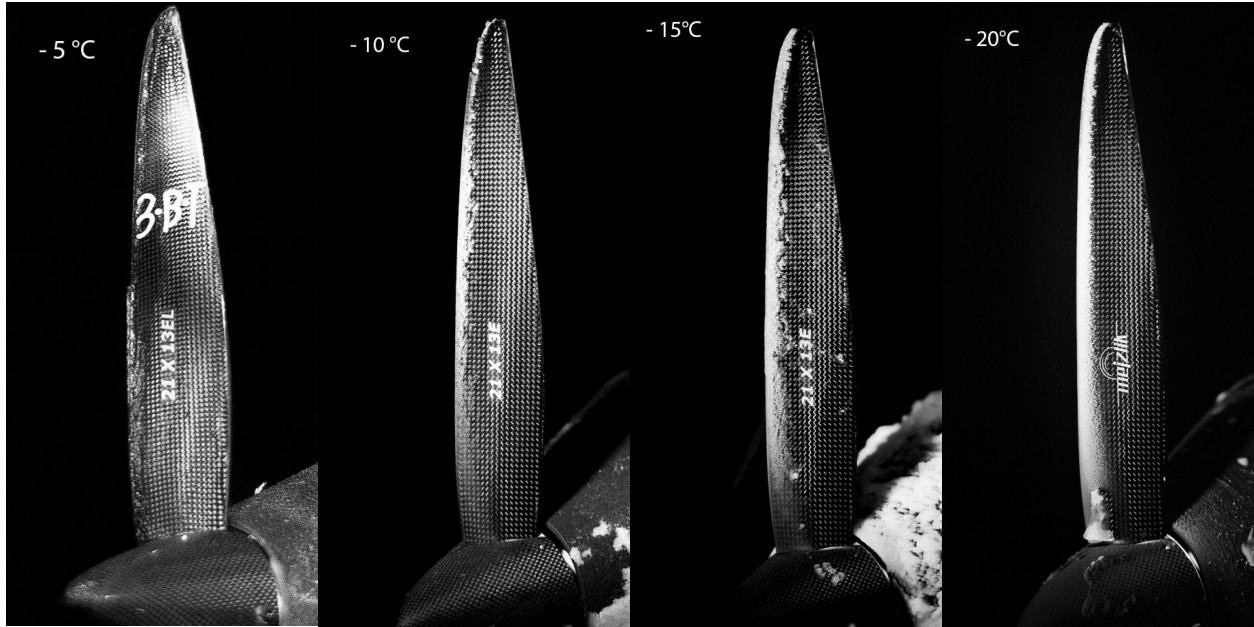


Fig. 9 Ice on the propeller after 60 s in icing conditions with an rotation rate of 4200 1/min, an LWC of 0.44 g/m³ and a wind velocity of 25 m/s. From left at -5 °C, -10 °C, -15 °C and -20 °C.

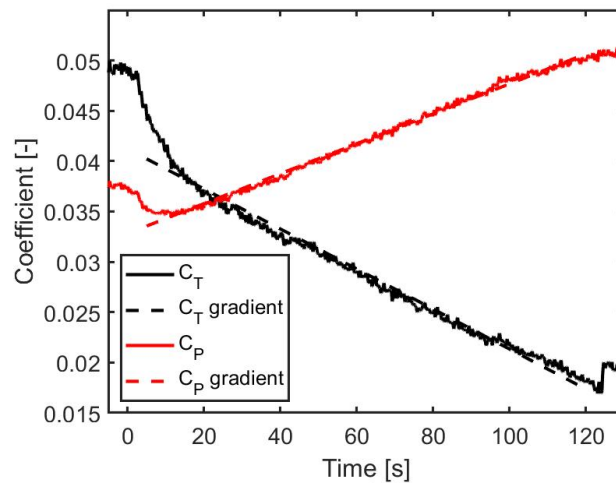


Fig. 10 Performance degradation on the propeller at -20 °C at an 5000 1/min an airspeed of 25 m/s and an LWC of 0.45 g/m³. The linear approximations of the coefficients are marked with dashed lines.

1. Change in the thrust coefficient

The results overall temperatures are plotted in Fig. 11, along with the approximation used in the model. The data is shown in a box plot, where the box shows the range between the upper and lower quartile. The horizontal line represents the median of the data. Outliers are detected as data points which are more than 1.5 the interquartile range apart from the box. The whiskers represent the range of the data points that are not considered outliers. It can be seen, that the gradient of the thrust loss is dependent on the temperatures, with a peak at -10. The measured performance degradation adheres well to the expected values. The second-order approximation shows a good agreement to the median values for each temperature.

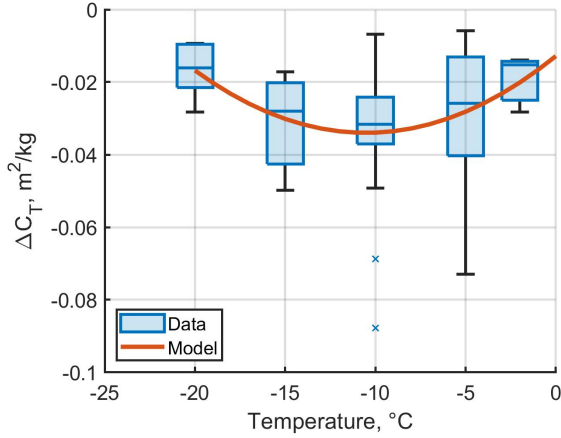


Fig. 11 Plot of the measured ΔC_T Values and the model values for different temperatures.

Table 3 Parameters for the ΔC_T estimation.

Parameter	Value [-]
$\Delta C_{T,2}$	0.00140
$\Delta C_{T,1}$	0.0254
$\Delta C_{T,0}$	0.0233

2. Change in the power coefficient

For the ΔC_P calculation, the relative increase in power was calculated for all experimental runs. The data points were selected after 10 s, 20 s, 30 s, 60 s, 90 s, 120 s, 180 s, 240 s, 300 s and 360 s, and averaged over one second. The reference value is taken from before the start of the spray system of the wind tunnel and averaged over 10 seconds. The gradient of the linear fitting curve was taken as ΔC_P at the temperature.

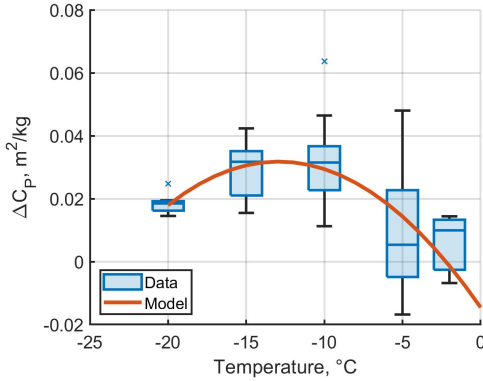


Fig. 12 Plot of the calculated ΔC_P values and the fitting curve through the data.

Table 4 Parameters for the ΔC_P estimation.

Parameter	Value [-]
$\Delta C_{p,0}$	-0.00890
$\Delta C_{p,1}$	-0.0166
$\Delta C_{p,2}$	-5.79e-04

E. Results of the model

The model was used to predict the performance of the propeller. First the performance of the propeller was analysed for different temperatures at a constant advance ratio. Here the model predicts a linear increase in the power coefficient until the ice shedding occurs. The LWC was set to 1 g/m² for the calculation. It can be seen in Fig. 13, that the lower the temperatures are, the steeper is the increase in the power coefficient and the larger is the amount of ice that can accumulate on the propeller until the ice shedding occurs.

Figure 14 presents the variation of the lift coefficient can be seen over the icing time for the same conditions. Here the decrease of the thrust coefficient is also linear. The steepness of the decrease is also dependent on the temperature, with the steepest decline at -10 °C. Since at -15 °C the adhesion forces on the ice are the stronger, more ice can accumulate and the final thrust coefficient is lower than at -10 °C after the ice shedding.

Both parameters can be combined to show the efficiency of the propeller as shown in Fig. 15. Here a similar structure emerges as when looking at the single parameters. The efficiency loss of the propeller is changing with the

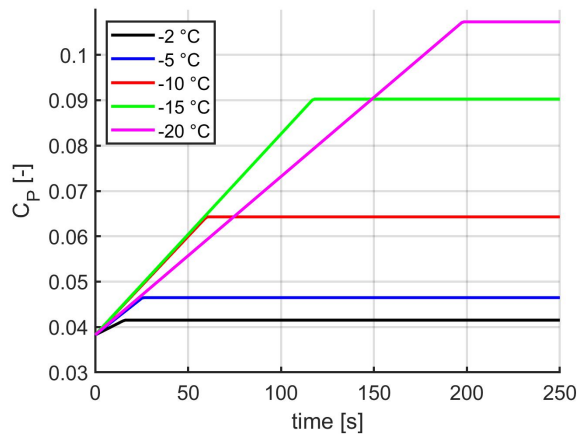


Fig. 13 Power coefficient of the Propeller for an advance ratio of $J = 0.6$ at different temperatures.

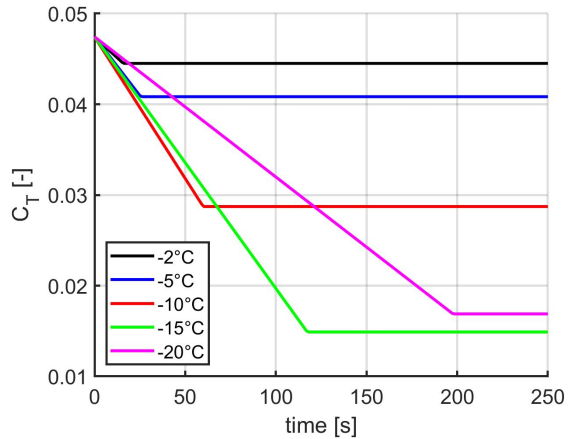


Fig. 14 Thrust coefficient of the Propeller at an advance ratio of $J = 0.6$ at different temperatures.

temperature. The final performance degradation is decreasing with the temperature. The higher thrust coefficient at -20°C is compensated by the increase in the power coefficient. Therefore the propeller degradation is the strongest here. -10°C shows the strongest gradient in the performance degradation until the ice starts shedding from the propeller.

This model also allows for the calculation of the polar of the propeller after a set amount of icing time. Here the amount of ice accretion was calculated for a set amount of time and the performance of the propeller over its entire polar is estimated. This is shown in Fig. 16. Here the performance of the propeller is shown after 60 s of ice accretion time and compared with the clean polar of the propeller. The performance of the propeller is impacted by a significant increase in the required power and a decrease in the created thrust.

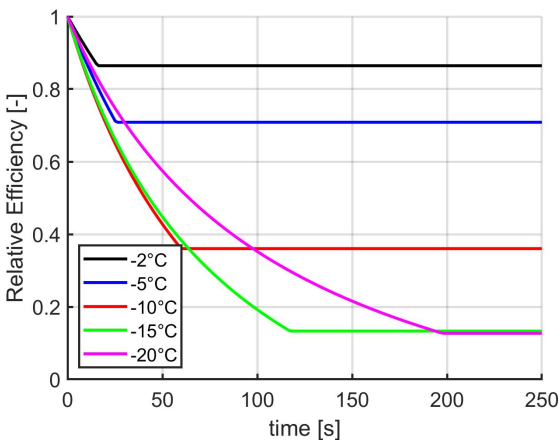


Fig. 15 Predicted efficiency of the propeller at a rotation rate of 4200 1/min and an LWC of 0.44.

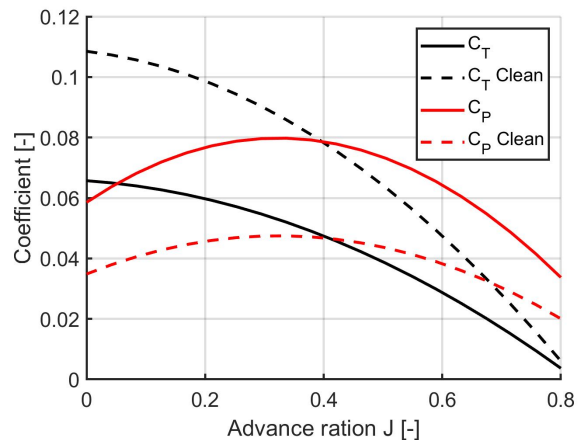


Fig. 16 Model prediction for the polar of the propeller after 120 s of icing at a LWC of 1 g/m^3 and an rotation rate of 4200 1/min.

IV. Discussion

A. Experimental Results

For this paper, multiple experiments were performed to analyse the impact of icing on the performance of a propeller of a UAV. The results of the tests show that the ice accretion is strongly correlated to the temperature. The amount of ice that can accumulate on the propeller seems to grow with decreasing temperatures. During the time of the ice accretion, the performance of the propeller is decreasing. A possible reason why more ice can accumulate on the propeller can be attributed to the adhesion forces on the propeller. The lower the ambient temperature is, the stronger the bond between the ice and the propeller. At $-2\text{ }^{\circ}\text{C}$ the time until the first ice shedding event is growing again. Looking at the images captured of the propeller at this temperature, it appears that the ice mass on the propeller is lower at those temperatures compared to lower temperatures. Therefore not all the water droplets impinging on the propeller freeze on the propeller. Another factor increasing the time until the ice is shedding is the rotation rate of the propeller. Lower rotation rates will reduce the centrifugal forces acting on the ice and thus increase the time until the ice is shedding. In addition to this, lower rotation rates of the propeller reduce the velocity of the air relative to the propeller blade and thus they will reduce the amount of water that will impinge on it at the same time. This is likely another factor increasing the time until the ice sheds off the propeller. Another factor that could play a role here is the impact of the chord length, the droplet size and the velocity on the ice shapes.

The experiments have shown that the ice will shed off the propeller in multiple sections, usually starting from the tip of the propeller. This amount of ice shedding is not always the same on both propeller blades, which leads to the generation of vibrations. This could be due to the uneven aerodynamic forces on the propeller blade and likely to a larger degree by the difference in the ice mass of both propeller blades. These vibrations pose a challenge to the collection of data on the performance of propellers during long experiments, as they can prevent the safe conduction of the experiments, and lead to a drift in the force measurement sensors.

The change in the lift and drag coefficient of the propellers seems to be dependent on the temperature. From the measured conditions $-10\text{ }^{\circ}\text{C}$ has been the worst case for the degradation of the performance. This can be observed when looking at the steepness of the performance degradation before the first ice shedding event. The reduced degradation could be explained by the different ice shapes at colder temperatures. Rime ice shapes generally observed at lower temperatures are associated with more streamwise ice shapes compared to glaze ice shapes. These ice shapes will lead to a reduced performance degradation compared to the more complex ice shapes presented with higher temperatures. Another reason could be found in the different ice accretion times. Since the ice accretion time, until the first ice shedding event, is longer for lower temperatures, this could influence the change in the average degradation of the propeller. The opposite is true for the measurements at $-5\text{ }^{\circ}\text{C}$. Here the ice accretion times are very short for all but the runs with very low rotation rates. Those short times complicate the reliable determination of the performance degradation gradient. When the spray system of the wind tunnel is started, the force and the torque measured drop by a significant margin. The propeller efficiency is unaffected by this, as both values drop in unison. The most likely explanation for the drops is that the airspeed increases due to the injection of air and water from the spray nozzles. Another explanation for the fast drop in the thrust coefficient would be the formation of a thin layer of ice on the propeller blade. This could lead to a change in the performance of the propeller by inducing the transition from a laminar boundary layer to a turbulent one. This could explain part of the loss of thrust, although this could be expected to lead to an increase in the torque rather than a decrease.

The experiments showed that the influence of ice on the propeller is dependent on the ice morphology. It has been shown that icing at $-10\text{ }^{\circ}\text{C}$ has the strongest influence on the performance of the propeller. One explanation for this behaviour could be the ice shape. At temperatures below $-10\text{ }^{\circ}\text{C}$ rime ice is formed on the propeller, which is a streamwise ice shape. While at higher temperatures mixed and glaze ice shapes are created. Glaze ice shapes create horns and complex geometries, which are more detrimental to the performance of the propeller. An explanation of the reduced impact of the icing on the propeller at high temperatures could be the freezing fraction of the ice on the propeller. The *TWC* is estimating the total water that is impinging on the propeller, but at higher temperatures, not all the water is freezing into ice. Parts of the water will shed from the propeller into the airflow again. The water could also run towards the back of the propeller and freeze there. But this behaviour was not observed during the experiments. This leads to a lower ice mass than expected and this, in turn, will reduce the calculated gradient of the propeller ice. In the presented structure, this shows up as an increase in the adhesion parameter of the ice at high temperatures, which could be explained by the reduced freezing fraction at those temperatures. Since the *TWC* is an estimation of the water that could be collected by the propeller, which includes the water that is not freezing, the actual ice mass is lower than the value used for the adhesion force estimation. This could lead to difficulties predicting the performance of propellers

at high temperatures. The change between the ice morphology and the freezing fractions is also dependent on the rotation rate of the propeller. Therefore the rotation rate of the propeller has an influence on the gradients, which could explain the large variation in the measurements at $-10\text{ }^{\circ}\text{C}$ and at $-5\text{ }^{\circ}\text{C}$. Since in this temperature range the ice morphology is changing from glaze to rime, everything that influences the ice morphology will have a large influence on the measurement.

B. Performance model

In the presented model, the ice accretion and the performance of the UAV propeller in icing conditions are estimated. The performance estimation using a polynomial approach provided a good estimation of the performance of the clean propeller.

In this paper, the ice accretion is estimated using an ice accretion parameter TWC that represents the amount of ice accumulated on the propeller. The ice accretion parameter is using the LWC and the relative airspeed. In this factor, the influence of the collection efficiency and the freezing fraction are not included. This could lead to a change in the actual ice accretion for changing propeller shapes or atmospheric conditions. By separating the cases for different temperatures, the change of the freezing fraction with the temperature is captured, but the effect of the Reynolds number on the freezing fractions is not captured.

The ice shape is important because it has a large influence on the aerodynamic forces acting on the ice shapes. The icing extend of the ice shape on the propeller influences the area that is connecting the ice and the propeller. A larger icing extend leads to a larger surface area for the bound between the ice and the propeller. This will allow the ice to stay attached longer to the propeller. In contrast to this, a lower icing extend will reduce the adhesion of the ice to the propeller. As the ice grows, the ice accumulation rate will be affected by the existing ice shape. growing horn ice shapes as observed for glaze and mixed conditions can increase the area on which droplets can be collected significantly and thus increase the ice accumulation rate very fast. The ice shedding estimation is performed for the outer part of the propeller. This seems to allow for a prediction of the first ice shedding event. For the estimation of the actual size of the ice block shed off the propeller, the analysis would have to be performed on multiple sections and the strength of the ice would have to be known. The collected ice mass on the propeller could be used to estimate an upper bound on the size of an ice block that could shed off the propeller. For this, the ice mass would have to be estimated over the thickness of the propeller. The proposed equations could be used to predict the icing on multiple parts of the propeller. The ice shedding model does not regard the ice shape that is created. The choice of the first ice shedding event as an indicator of the final performance degradation prevents the calculation of the performance of a propeller after partial ice shedding. As the center of the propeller will continue to accumulate ice, it is possible that at a later stage the propeller will have a stronger performance degradation. As the areas where ice has been shed will start to accumulate new ice again, a theoretical worst case would be if the previous ice shedding event stagger in a way as to have the ice on the entire length of the propeller leading edge is shedding at once. Another factor that is not considered is the ice accumulation in other areas than the leading edge of the propeller. Small amounts of ice will accumulate on the pressure side of the propeller, and this ice will not follow the same ice shedding cycles as the ice on the leading edge of the propeller. Ice shedding could also be represented by reducing the calculated amount of ice on the propeller. This could allow for an analysis of the dynamic forces created by the ice shedding on the flight stability and the control response of an autopilot. This would be especially interesting for multi-rotor UAVs.

The linear approximation of the thrust and the power coefficients over the ice accretion time appears to be a good fit for the estimation of the coefficients for short icing events. For cases with a very long ice accretion time, the gradient of the thrust coefficient decreases with the ice accretion time, which would make an exponential fit function another good fit for this coefficient. The reason for this behaviour might be in the relationship between the thrust coefficient and the induced velocity of the propeller. As the thrust decreases, the induced air velocity is also decreasing. This leads to an increase in the local angle of the propeller blade and could thus explain the behaviour of the propeller. Another reason is that the drag the propeller can produce is limited, which sets a lower limit on the value C_T can reach after a long ice accretion. The propeller polar of the iced and the ice-free propeller shows that the iced thrust coefficient over advance ratio can be reasonably be approximated by a linear factor. The power coefficient on the other hand shows an different behaviour, and the gradient is lower with the intersection of the power coefficient moved towards a higher advance ratio. So the linear approximation is only valid in a small range around the advance ratio at which the experimental data was collected.

The use of a second-order approximation for the degradation limits the use of the model to the temperature range for which data has been collected. In this paper, this is up to $-20\text{ }^{\circ}\text{C}$. It is not expected that the reduction of the impact of the

ice on the performance of the propeller will not turn into a benefit, as the model would suggest for temperatures below $-20\text{ }^{\circ}\text{C}$. Once the temperature falls low enough so that all the water freezes immediately in contact with the propeller, the ice shape is no longer strongly correlated with the temperature. Therefore for temperatures below $-20\text{ }^{\circ}\text{C}$ the coefficients at $-20\text{ }^{\circ}\text{C}$ could be used for the estimation of the performance loss of the propeller until further data is gathered.

Other factors that influence the ice accretion can be separated into conditions of the environment or of the propeller. External factors that are not included are the median volume diameter of the droplets. This influences the ice shapes and the freezing fractions of the propeller. While the *LWC* is included in the model, the influence of the *LWC* on the ice shape is not captured. These factors are very important for the estimation of the model, as they can affect the same propeller in different conditions. Including them would increase the ability of the model to capture the performance in different icing conditions. Another set of factors that affect the performance impact of the icing are dependent on the shape of the propeller. They are the material of the surface, the surface roughness or the leading edge radius and the chord length. Including them would increase the ability of the model to estimate the propeller performance of different propellers. The model can estimate the performance of different propellers. To change the estimated propeller performance the parameters for the clean propeller estimation have to be replaced by the parameters of the new propeller. If the propeller has a different material, a change in the adhesion to the surface is to be expected. And if the diameter changes, it is likely that the performance degradation slope will change as well, as the thickness of the ice relative to the chord length is now different, which influences the impact the ice has on the performance. Also, the impact of the rising stagnation temperature with increasing propeller diameters or rotation rates will change the way ice accumulates on propellers.

V. Outlook

With future work, the model could be expanded to cover the performance of the propeller more completely. One area which would lend itself to expansion is the influence of the rotation rate and the advance ratio of the propeller on the ice shapes. The different ice morphology will change the ice shape and henceforth the influence the ice has on the performance of the propeller. When the propeller turns faster the temperatures at which glaze, mixed or rime ice forms will shift to lower temperatures. A change in the advance ratio when the ice accumulates on the propeller will influence the position of the stagnation point on the propeller and thus the position and the shape of the ice shape. This will influence the way the ice influences the performance of the propeller. Another option for further work is to replace the ambient temperature as a scaling factor by the stagnation temperature. This would include the change in rpm better into the model. Lastly, focusing on the influence of the chord length of the propeller on the performance impact would allow for a greater application of the model for different propellers.

The shown relationship between the ice shedding time and the rotation rate of the propeller can be exploited for the protection of the propeller of a UAV from ice, by increasing the rotation rate of the propeller. This will lead to a reduction in the maximum performance penalties from icing as the ice will shed earlier with lower performance losses. For operations at very low temperatures, the use of a system to protect the propeller from icing is required to keep the UAV operating. The loss in propeller performance will occur at the same time during which the ice accumulation on the airframe will reduce the lift and increase the drag of the UAV. Therefore it would require an increase in the thrust of an unprotected UAV to keep the UAV flying.

VI. Conclusion

In this paper, the impact of icing on the performance of the propeller of a fixed-wing UAV is presented. The propeller shows a large reduction in the thrust of the propeller and an increase in the torque of the propeller. The results show that the ice shedding is a function of the temperature. The lower the temperature gets, the later the first ice shed is occurring. The gradient of the thrust and torque coefficients shows a maximum at $-10\text{ }^{\circ}\text{C}$. The maximum performance degradation is seen at $-20\text{ }^{\circ}\text{C}$. Therefore these temperatures are the most critical for the operation of UAVs, and an icing protection system for propellers of UAVs should be designed for those conditions. The results are used to develop a model to predict the performance of the propeller during its operational envelope. A method was developed to analyse and compare the results of the ice accretion on a propeller in an icing wind tunnel. The model predicts the ice accumulation on the propeller and models the ice shedding. Using the ice accumulated on the propeller the performance of the propeller is predicted. The methodology can be used to compare different experiments that are performed on different propellers to compare the differences in the ice accretion and ice shedding between different conditions.

Acknowledgments

The work is partly sponsored by the Research Council of Norway through the Centre of Excellence funding scheme, project number 223254, AMOS, and an Industrial PhD with project number 321667, project BIA Rotors with project number 296228, and project IKTPLUSS with project number 316425. We also thank Mejzlik for their cooperation.

References

- [1] Cao, Y., Tan, W., and Wu, Z., "Aircraft icing: An ongoing threat to aviation safety," *Aerospace Science and Technology*, Vol. 75, 2018, p. 353–385. <https://doi.org/10.1016/j.ast.2017.12.028>.
- [2] Hann, R., and Johansen, T., "Unsettled Topics in Unmanned Aerial Vehicle Icing," *SAE International, SAE EDGE Research Report EPR2020008*, 2020. <https://doi.org/10.4271/epr2020008>.
- [3] Gent, R. W., Dart, N. P., and Cansdale, J. T., "Aircraft Icing," *Philosophical Transactions: Mathematical, Physical and Engineering Sciences*, Vol. 358, No. 1776, 2000, pp. 2873–2911. URL <http://www.jstor.org/stable/2666834>.
- [4] Siquig, R., "Impact of Icing on Unmanned Aerial Vehicle (UAV) Operations," *Technical report, Naval Environmental Prediction Research Facility*, 1990.
- [5] Szilder, K., and McIlwain, S., "In-Flight Icing of UAVs - The Influence of Reynolds Number on the Ice Accretion Process," *SAE Technical Paper Series*, 2011. <https://doi.org/10.4271/2011-01-2572>.
- [6] Fajt, N., Hann, R., and Lutz, T., "The Influence of Meteorological Conditions on the Icing Performance Penalties on a UAV Airfoil," *8th European Conference for Aeronautics and Space Sciences (EUCASS)*, 2019.
- [7] Hann, R., Hearst, R. J., Sætran, L. R., and Bracchi, T., "Experimental and Numerical Icing Penalties of an S826 Airfoil at Low Reynolds Numbers," *Aerospace*, Vol. 7, No. 4, 2020, p. 46. <https://doi.org/10.3390/aerospace7040046>.
- [8] Williams, N., Benmeddour, A., Brian, G., and Ol, M., *The Effect of Icing on Small Unmanned Aircraft Low Reynolds Number Airfoils*, 2017. URL <https://search.informit.org/doi/10.3316/informit.738050435297237>.
- [9] Liu, Y., Li, L., Ning, Z., Tian, W., and Hu, H., "Experimental investigation on the dynamic icing process over a rotating propeller model," *Journal of Propulsion and Power*, Vol. 34, No. 4, 2018, pp. 933–946. <https://doi.org/10.2514/1.B36748>.
- [10] Liu, Y., Li, L., Chen, W., Tian, W., and Hu, H., "An experimental study on the aerodynamic performance degradation of a UAS propeller model induced by ice accretion process," *Experimental Thermal and Fluid Science*, Vol. 102, No. November 2018, 2019, pp. 101–112. <https://doi.org/10.1016/j.expthermflusci.2018.11.008>, URL <https://doi.org/10.1016/j.expthermflusci.2018.11.008>.
- [11] Müller, N., Hann, R., and Lutz, T., *UAV Icing: Numerical Simulation of Propeller Ice Accretion*, AIAA AVIATION 2021 FORUM, 2021. <https://doi.org/10.2514/6.2021-2673>, URL <https://arc.aiaa.org/doi/abs/10.2514/6.2021-2673>.
- [12] Yan, S., Opazo, T. I., Langelaan, J. W., and Palacios, J. L., "Experimental Evaluation and Flight Simulation of Coaxial-rotor Vehicles in Icing Clouds," *Journal of the American Helicopter Society*, 2019.
- [13] Hovenburg, A. R., de Alcantara Andrade, F. A., Hann, R., Rodin, C. D., Johansen, T. A., and Stovold, R., "Long-Range Path Planning Using an Aircraft Performance Model for Battery-Powered sUAS Equipped With Icing Protection System," *IEEE Journal on Miniaturization for Air and Space Systems*, Vol. 1, No. 2, 2020, p. 76–89. <https://doi.org/10.1109/jmass.2020.3003833>.
- [14] Frimann Loes Narum, E., Hann, R., and Arne Johansen, T., "Optimal Mission Planning for Fixed-Wing UAVs with Electro-Thermal Icing Protection and Hybrid-Electric Power Systems," *2020 International Conference on Unmanned Aircraft Systems (ICUAS)*, 2020. <https://doi.org/10.1109/icuas48674.2020.9214054>.
- [15] Hann, R., Enache, A., Nielsen, M. C., Stovner, B. N., van Beeck, J., Johansen, T. A., and Borup, K. T., "Experimental Heat Loads for Electrothermal Anti-Icing and De-Icing on UAVs," *Aerospace*, Vol. 8, No. 3, 2021, p. 83. <https://doi.org/10.3390/aerospace8030083>.
- [16] Hann, R., Borup, K., Zolich, A., Sorensen, K., Vestad, H., Steinert, M., and Johansen, T., "Experimental Investigations of an Icing Protection System for UAVs," *SAE Technical Paper Series*, 2019. <https://doi.org/10.4271/2019-01-2038>.
- [17] Hann, R., Wenz, A., Gryte, K., and Johansen, T. A., "Impact of atmospheric icing on UAV aerodynamic performance," *2017 Workshop on Research, Education and Development of Unmanned Aerial Systems (RED-UAS)*, 2017. <https://doi.org/10.1109/red-uas.2017.8101645>.

- [18] Cheung, M. C., Hann, R., and Johansen, T. A., "UAV Icing: A Unified Icing Severity Index Derived from Performance Degradation," (*In Press AIAA Aviation 2022*), 2022.
- [19] Tiihonen, M., Jokela, T., Makkonen, L., and Bluemink, G.-J., "VTT icing wind tunnel 2.0," *Winterwind International Wind Energy Conference*, 2016.
- [20] Mejlík, "Propeller 21X13 CCW 2B E - Mejlík Propellers," *shop.mejlik.eu* (*Accessed 02.11.2021*), 2021. URL <https://shop.mejlik.eu/propeller-21x13-ccw-2b-e/>.
- [21] "RCBENCHMARK series 1780 test stand - tyto robotics," *Tyto Robotics Inc* (*Accessed 02.11.2021*), 2021. URL <https://www.tytorobotics.com/pages/series-1780>.
- [22] "Calibration and Acceptance of Icing Wind Tunnels," "*AC-9C Aircraft Icing Technology Committee*", 2015. <https://doi.org/https://doi.org/10.4271/ARP5905>, URL <https://doi.org/10.4271/ARP5905>.
- [23] McCormick, B., *Aerodynamics, Aeronautics, and Flight Mechanics*, 2nd ed., Wiley, 1994.
- [24] Coates, E. M., Wenz, A., Gryte, K., and Johansen, T. A., "Propulsion System Modeling for Small Fixed-Wing UAVs," *2019 International Conference on Unmanned Aircraft Systems (ICUAS)*, IEEE, 2019, pp. 748–757.
- [25] Tarquini, S., Antonini, C., Amirfazli, A., Marengo, M., and Palacios, J., "Investigation of ice shedding properties of superhydrophobic coatings on helicopter blades," *Cold Regions Science and Technology*, Vol. 100, 2014, pp. 50–58. <https://doi.org/https://doi.org/10.1016/j.coldregions.2013.12.009>, URL <https://www.sciencedirect.com/science/article/pii/S0165232X13002085>.
- [26] Clancy, L., *Aerodynamics*, A Halsted Press book, Wiley, 1975. URL <https://books.google.no/books?id=zaNTAAAAMAAJ>.
- [27] Mohamed, A., and Farzaneh, M., "An experimental study on the tensile properties of atmospheric ice," *Cold Regions Science and Technology*, Vol. 68, No. 3, 2011, pp. 91–98. <https://doi.org/https://doi.org/10.1016/j.coldregions.2011.06.012>, URL <https://www.sciencedirect.com/science/article/pii/S0165232X11001145>.
- [28] Druetz, J., Phan, C., Laforte, J., and Nguyen, D., "The Adhesion of Glaze and Rime on Aluminium Electrical Conductors," *Transactions of the Canadian Society for Mechanical Engineering*, Vol. 5, No. 4, 1978, pp. 215–220. <https://doi.org/10.1139/tcsme-1978-0033>, URL <https://doi.org/10.1139/tcsme-1978-0033>.
- [29] Han, Y., Palacios, J. L., and Smith, E. C., "An experimental correlation between rotor test and wind tunnel ice shapes on NACA 0012 airfoils," *SAE Technical Papers*, 2011. <https://doi.org/10.4271/2011-38-0092>.